Atmospheric
Measurement
Techniques

Development and validation of satellite-derived surface NO$_2$ estimates using machine learning versus traditional approaches in North America

Debora Griffin[1], **Colin Hempel**[1,2], **Chris McLinden**[1,3], **Shailesh Kumar Kharol**[4], **Colin Lee**[1], **Andre Fogal**[1,5], **Christopher Sioris**[1], **Mark Shephard**[1], and **Yuan You**[1]

[1]Air Quality Research Division, Environment and Climate Change Canada, Toronto, Ontario, Canada
[2]Department of Physics, University of British Columbia, Vancouver, Canada
[3]Department of Physics and Engineering Physics, University of Saskatchewan, Saskatoon, Saskatchewan, Canada
[4]AtmoAnalytics Inc., Brampton, Canada
[5]Department of Physics and Astronomy, University of Waterloo, Waterloo, Canada

Correspondence: Debora Griffin (debora.griffin@ec.gc.ca)

Abstract. Nitrogen dioxide (NO$_2$) is one of the key pollutants with profound implications for air quality, and human health, and is needed to establish the air quality health index (AQHI). Currently, over 600 surface air monitoring stations are distributed across Canada and the United States measuring NO$_2$, but many areas remain unmonitored leading to incomplete information for health risk assessments. This study leverages Tropospheric Monitoring Instrument (TROPOMI) satellite observations and machine learning models to derive high-resolution surface NO$_2$ concentrations, provides enhanced spatial coverage and accuracy, revealing urban-rural NO$_2$ gradients across North America. Existing traditional methods rely on scaling with modeled profiles to obtain NO$_2$ surface concentrations from satellite observations. Here, we compare this traditional method to a machine learning approach that utilizes NO$_2$ observations from TROPOMI, together with meteorological parameters, land cover type, topography, and emission inventories. Our results show that the machine learning (using random forest) yields less bias between the surface monitoring measurements and the "satellite-derived" surface concentrations, significantly improved the correlation coefficient ($R^2 \sim 0.77$–0.91) compared to the traditional method ($R^2 \sim 0.39$–0.57) and yields to significantly less bias.

1 Introduction

Nitrogendioxide (NO$_2$) is a highly reactive gas that is a major component of outdoor air pollution. It is primarily produced by combustion processes, including burning fossil fuels in motor vehicles, power plants, and industrial processes. NO$_2$ can also be formed through natural processes such as lightning and microbial activity in soils. NO$_2$ plays a significant role in the production of tropospheric ozone and has adverse effects on the environment and human health. Exposure to high levels of NO$_2$ can cause a range of adverse health effects, particularly on the respiratory system (Health Canada, 2024; Environment Canada, 2024). As such it is often included in the calculation of air quality indices, a metric which communicates the health risk associated with pollution levels in ambient air. Some examples include the US Air Quality Index, the Air Quality Health Index in Canada, the European Air Quality Index, and the National Air Quality Index in India.

NO$_2$ is one of several air pollutants regulated by national and international air quality standards, and efforts to reduce NO$_2$ emissions from transportation and industry are an important part of air quality management strategies. Satellite

and ground-based measurements have shown significant progress in the reduction of NO$_2$ emissions, including across the US and Canada (Russell et al., 2012; Kharol et al., 2015). Surface concentrations are monitored in Canada through the National Air Pollution Surveillance Program (NAPS; https://www.canada.ca/en/environment-climate-change/services/air-pollution/monitoring-networks-data/national-air-pollution-program.html, last access: 19 November 2025), with the mission to provide accurate and long-term air quality data across Canada. Currently, there are roughly 290 NAPS NO$_2$ monitoring stations. The equivalent in the US is the Air Quality System (AQS) operated by the Environmental Protection Agency (EPA) (https://www.epa.gov/outdoor-air-quality-data, last access: 19 November 2025), which has approximately 450 NO$_2$ monitoring stations at present. Even with several hundred monitoring stations across Canada and the US, there remains wide monitoring gaps, especially in more remote areas and smaller communities.

Satellite observations can help to fill some of these gaps with previous studies showing the capability of satellite observations to detect ground-level NO$_2$ (Goldberg et al., 2021; Jeong and Hong, 2021). However, these satellite-based sensors observe vertical column densities (VCDs) rather than just the near-surface concentrations. but rather NO$_2$ through the entire atmospheric column. VCDs from the Tropospheric Monitoring Instrument (TROPOMI), a satellite sensor show a strong correlation with surface concentrations, indicating some sensitivity near the surface, which allows for the inference of surface concentrations (Goldberg et al., 2021; Jeong and Hong, 2021). There are several ways to infer surface concentrations from satellite observations. Traditionally, model scaling is a common approach where a ratio between model surface and model VCDs is applied to the satellite VCDs (Lamsal et al., 2008; McLinden et al., 2014; Kharol et al., 2015; Griffin et al., 2019; Cooper et al., 2020). This heavily relies on the accuracy of the air quality model or chemical transport (CTM) model and the winds that drive the model, and can introduce errors when the location of the emissions or the wind direction and speed used by the CTM model is not correct. More recently, machine learning has become more popular with the advancement of new technologies. When used with caution, machine learning is a powerful tool that can analyze large datasets and identify patterns that are not easily recognizable by humans. There have been several studies on using machine learning (ML) algorithms with TROPOMI NO$_2$ tropospheric columns to generate surface NO$_2$ concentrations in different parts of the world, including China (Long et al., 2022; Grzybowski et al., 2023), and Germany (Chan et al., 2021). Further information specifically on studies using machine learning to obtain surface NO$_2$ from satellite observations can be found in Siddique et al. (2024). However, to our knowledge, few studies have focused on applying such methods in less populated regions such as Canada. This gap is significant because the condi-

tions in Canada differ significantly from those in densely populated regions: surface monitoring networks are sparser, emission sources are different compared to urban areas, and the limited spatial extent of measurement networks in northern Canada contribute to the challenge. These differences highlight the need to adapt and evaluate ML approaches under these conditions.

The goal of this work is to develop a ML-based surface NO$_2$ product that is reliable for both near-real time monitoring as well as for retrospective environmental and health impact studies. Here, we compare our machine learning with the traditional method of obtaining surface concentrations from satellite observations in North America, and highlight some of the relevant challenges. Our dataset of NO$_2$ surface concentrations is publicly available to download https://hpfx.collab.science.gc.ca/~deg001/surfaceNO2 (last access: 19 November 2025).

2 Datasets and Methodology

2.1 TROPOMI NO$_2$

TROPOMI (TROPOspheric Monitoring Instrument) is a satellite instrument designed to observe the nitrogen dioxide (NO$_2$) in the troposphere (Hu et al., 2018; Veefkind et al., 2012). It is part of the European Space Agency's (ESA) Sentinel-5 Precursor mission, which aims to provide accurate and reliable atmospheric composition information for air quality and climate change. TROPOMI is a hyperspectral imaging spectrometer that operates in the ultraviolet, visible, near-infrared, and shortwave infrared spectral regions. It uses a push-broom scanning technique to capture high spatial-resolution images of the Earth's atmosphere in the UV-visible with a ground resolution of up to 3.5 km $\times$ 5.5 km (since August 2019, 7 km $\times$ 5.5 km prior). This provides the possibility of detecting and estimating NO$_2$ emissions, including urban and industrial regions (Griffin et al., 2019; Goldberg et al., 2019, 2024), shipping lanes (Riess et al., 2022), and power plants (Beirle et al., 2019; Dix et al., 2022). In this study we use version 2 of the NO$_2$ TROPOMI dataset (v2) and remove observations that have a quality flag below 0.75. Additionally, points over water are not presented in this study. While the surface concentrations are available for each TROPOMI observation, the learning-derived NO$_2$ surface concentrations over water are not shown here because their validity could not be verified in the absence of monitoring stations.

2.2 Air Quality Monitoring Stations

US and Canadian NO$_2$ from surface monitoring stations are used for two purposes: a portion is used to train the ML system while the remainder is used to evaluate the ML product.

The U.S. Environmental Protection Agency (EPA) has established a national network of air quality monitoring sta-

tions to measure various air pollutants, including NO$_2$. These monitoring stations are part of the EPA's Air Quality System (AQS) and provide hourly measurements of NO$_2$ concentrations at the surface level. The EPA's NO$_2$ monitoring network consists of approximately 450 sites in the United States. Similarly, in Canada, the National Air Pollution Surveillance (NAPS) program is a national network of air quality monitoring stations. The NAPS program has established a network of approximately 290 air quality monitoring stations across Canada.

The NO$_2$ measurements obtained by the AQS and NAPS networks are collected using chemiluminescence-based analyzers, which measure the concentration of NO$_2$ in the ambient air. These instruments operate alternately in nitric oxide (NO) and NO$_x$ mode, and the NO$_2$ concentrations are inferred indirectly as the difference between measurements obtained in the NO$_x$ mode and NO mode. Due to interference from other reactive nitrogen species, such as peroxyacetyl nitrate (PAN), nitric acid (HNO$_3$), nitrous acid (HONO), and organic nitrates, the NO$_2$ concentrations can be overestimated by the chemiluminescence-based analyzers (Winer et al., 1974; Demerjian, 2000; Steinbacher et al., 2007). Previous studies have accounted for this by applying a correction using modeled PAN, HNO$_3$, and alkyl nitrates (Lamsal et al., 2008, 2010; Kharol et al., 2015). In recent years, there have been advancements made to improve the accuracy of the NO$_2$ concentrations measured with these instruments, including selective catalytic reduction, scrubbers, and improved calibration. Thus, we have not applied a correction term to the NAPS and AQS NO$_2$ dataset.

To establish the training dataset, we calculate the 12:00–15:00 average – a time range representative of the TROPOMI overpass – for all the in situ NO$_2$ measurements over US and Canada for the time period between 2018 and 2022 (except in Sect. 3.1 we use 2018–2021 for training, as 2022 is used for validation). The location of the stations is shown in Fig. 1 with AQS as blue (450 sites) and NAPS (239 sites) as red points. This map also shows the locations of the model points (gray points, 290 sites) used (as further discussed in Sect. 3.2). A similar amount of synthetic background stations as NAPS stations is needed for the machine learning model to improve in background areas.

2.3 Machine Learning and Training methods

In this study, we use machine learning models to obtain surface concentrations for each TROPOMI observation (L2) on the same spatial resolution as the satellite observations themselves. To predict surface level NO$_2$, we utilize the machine learning algorithms in python sklearn (Breiman, 2001). As part of this study, we tested several machine learning methods, including neural networks, decision tree, and random forest. In this study, we found that the random forest led to the best results by far, leading to correlations around

$R^2 \sim 0.8$ between estimated daily mid-day and measured NO$_2$ surface concentrations (see Sect. 3).

The random forest machine learning algorithm (Breiman, 2001) consists of a random collection of decision trees and is trained on random subsets of features and data. The strength of this method is its robustness, simple implementation and its accountability for non-linearity making it a good option for the estimation of surface NO$_2$ concentrations from satellite observations. The trainable parameters in a random forest model are the input covariates and the thresholds at which they are split. The main hyperparameters in the random forest model are the number of trees in the random forest, the loss function or evaluation criterion used to assess the improvement training makes to the regression, the maximum number of splits a tree can have, and the maximum depth of the trees in the forest.

Since the method can be prone to over-fitting, it is important to select the model hyperparameters carefully, in order to obtain the best performance without overfitting the training data. Overfitting occurs when the model accurately predicts the training data but performs poorly on new data that was unseen during training. We split the data randomly into 90 % training and 10 % testing data to find the optimal hyperparameters. We trained random forests on the 90 % of the data multiple times, iterating through a range of values for the hyperparamters. The selected hyperparameters are the ones that maximize the average R^2 on both the training dataset and the unseen test data while ensuring that the difference between the testing and training R^2 is small (indicating that the model has not overfit the training data and generalizes well to unseen data). There is no generally accepted definition of "small" so we chose a threshold of 0.1. At this location in the hyperparameter space, the test R^2 value is not very sensitive to small changes in any of the hyperparameters. The final hyperparamters we used are presented in Table 1, further details on the impact of the hyperparameters on the correlation of the testing and training dataset can be found in the appendix (Fig. A1).

After hyperparameter tuning using the 10-fold cross validation method, we checked the performance of the model by splitting the available data into a training set encompassing the first 3 years (2019–2021) of data and a test set using only the 2022 data. We trained a random forest model using the best hyperparameters obtained above on the training set without letting the training see the test set. The spread of the R^2 between the training and test sets is then an indication of how much overfitting is happening. This training gave an $R^2_{\text{test}} = 0.78$ on the unseen 2022 data, while the average $R^2_{\text{training}} = 0.84$ for the 2019–2021 data, indicating a low degree of overfitting. This gives confidence that the model is not simply regurgitating the training data and can be safely used for predictions in areas and time periods away from the training dataset.

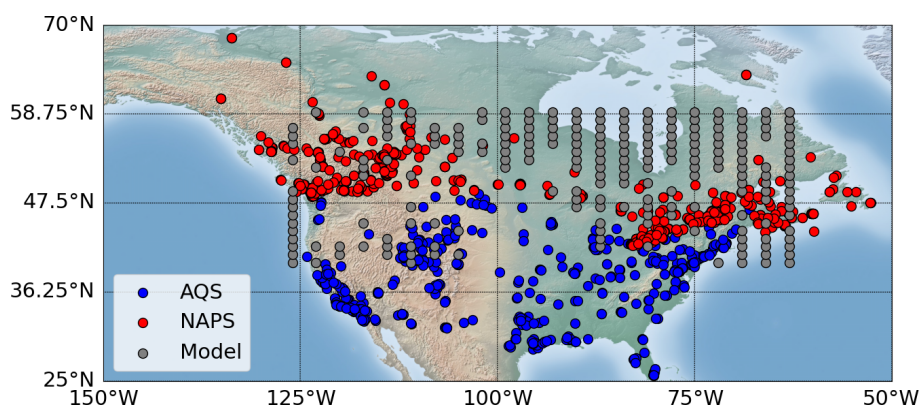Finally, for the random forest predictions presented here, we used the same hyperparmaters and trained a model on all

Figure 1. Location of the AQS (blue points) and NAPS (red points) stations that provide NO$_2$ surface concentration measurements. Also shown is the location of additional model output used for the training of the random forest algorithm (grey points).

Table 1. Hyperparameters tested and selected for the training of the machine learning algorithm.

Hyperparameter	Range	Selected Value
max_depth	1–100	16
n_estimators	1–100	30
min_samples_split	1–20	5
min_samples_leaf	1–10	2

4 years of available data to provide the best possible random forest model.

2.4 Input Parameters

To obtain the random forest fitting function, a training and test dataset needs to be established that consists of input parameters X and one output parameter Y. In our case the surface NO$_2$ measurements is the output parameter Y. For our final function we use the input parameters as listed in Table 2. Other parameters, including the ERA5 meteorological variables of 2 m surface temperature, total precipitation, relative humidity and the 2 m dew point temperature, as well as the CO emissions have been tested in our random forest fitting. However, since none of these had a significant impact on the correlation (less than 0.005) they were consequently removed to avoid over-fitting and to reduce the computational burden. Additionally, we tested including the location (longitude and latitude) of the stations (see Fig. A2), and while this overall improved the correlation, flaws started to appear when looking at maps containing locations that were not included in the training. Further details are discussed in Sect. 3.3.

2.4.1 ERA5 meteorology

Meteorology is an important component for an accurate prediction of surface concentrations. For example, the bound-

ary layer height can determine the amount of NO$_2$ near the surface relative to the total column, as well as wind speed and direction can impact the column to surface concentration ratio. For this reason we included 10 m winds, vertical velocity, surface pressure, and boundary layer height, from the European Centre for Medium-Range Weather Forecasts (ECMWF) ERA5 reanalysis (Dee et al., 2011) which is available hourly on 0.25×0.25 degrees resolution. Additionally, we tested using ERA5's 2 m temperature, the 2 m dew point temperature, total precipitation, and relative humidity, but found that it did not impact the correlation and had little effect on the random forest model. The ERA5 reanalysis data are interpolated to the nearest grid cell of the station/TROPOMI observation location. The meteorological parameters are averaged for the same hours as the insitu data (13:00 to 15:00 local time) for the training dataset and the closest hour is used for the TROPOMI L2 estimated surface observations. ERA5 was chosen over ERA-Land (which has the advantage of a higher spatial resolution), because it is available for each TROPOMI observation, and surface concentrations over water could be obtained.

2.4.2 Emission inventory

Including emissions inventory in the training of the model can help to pin-point location of elevated surface NO$_2$ concentrations thus we included the emissions of NO, NO$_2$, SO$_2$, and NH$_3$ in the machine learning algorithm. While the NO$_2$ and NO emissions are directly related to the NO$_2$ surface concentration, other pollutants can be helpful in the machine learning model as well. SO$_2$ emissions are typically an indicator of industrial activity, such as refineries potentially affecting the surface NO$_2$ concentrations differently compared to urban emissions. While NH$_3$ emissions are typical indicators of agricultural and some industrial activities nearby, NH$_3$ can also impact the formation NO$_x$ (Pai et al., 2021). The importance of the various parameters is discussed in Sect. 3 (Fig. 3). We use the same emission inventory as utilized in

Table 2. Input parameters used for the training of the machine learning algorithm. Some parameters are constant while others change hourly, however since TROPOMI only observes at mid-day, only coincident points with the TROPOMI observations are selected and indicated by "daily/mid-day" in the Table below.

Dataset	Parameter	Frequency	Resolution	Source
NO$_2$ surface observations	output/training	daily/mid-day	–	AQS and NAPS
TROPOMI	NO$_2$ tropospheric columns	daily/mid-day	$3.5 \times 5.5\,\text{km}^2$	Copernicus
Meteorology	10 m winds (zonal and meridional), vertical velocity, surface pressure, boundary layer height (BLH)	daily/mid-day	$0.25 \times 0.25°$	ERA5
Emissions	NO, NO$_2$, SO$_2$, NH$_3$	daily/mid-day	$10 \times 10\,\text{km}^2$	GEM-MACH
Topography	Elevation	constant	$10 \times 10\,\text{km}^2$	
Landuse	IGBP landuse classification	constant	$0.05 \times 0.05°$	MODIS MCD12Q1.061
population density	GPW dataset (2020 projection)	constant	$0.025 \times 0.025°$	Doxsey-Whitfield et al. (2015)
Temporal info.	month	–	–	–

the Environment and Climate Change Canada's (ECCC's) operational regional air quality model Global Environmental Multi-scale – Modelling Air quality and CHemistry (GEM-MACH). These emissions are on a 10 km × 10 km resolution in Canada and the US and vary by hour, day of the week and month. The operational forecast makes use of 2013 emissions information and provides updated projections of emissions for 2023 in the US and Mexico and 2020 in Canada (Zhang et al., 2018). The emissions used in the model are processed using the Sparse Matrix Operator Kernel Emissions (SMOKE) (Coats, 1996). For each measurement station, or TROPOMI location, the emissions of the closest grid box are used for the coincident time.

2.5 GEM-MACH model

Output from the GEM-MACH model is used in two ways in this study: (1) for the traditional scaling method, and (2) to provide surface concentrations for synthetic "stations" in remote areas (more details in Sect. 3.2). The operational version of the model (Moran et al., 2010; Pendlebury et al., 2018) has a $10 \times 10\,\text{km}^2$ grid cell size for North American domain, a 2-size bin aerosol size distribution and 42 trace gases and eight particle species. GEM-MACH provides hourly output for a North American modeling domain with an internal "physics" time step of 7.5 min. The chemical components of GEM-MACH reside as a subroutine package within the model's meteorological physics model, the latter a component of the Global Environmental Multiscale (GEM) weather forecast model (Côté et al., 1998; Girard et al., 2014). The operational model run is "initialized", meaning the meteorological parameters are replaced by analysis every 12 h, at 00:00 and 12:00 UTC. Further details on

GEM-MACH can be found in, Makar et al. (2015b, a) and Akingunola et al. (2018).

2.6 Traditional scaling method

In previous studies, e.g. Lamsal et al. (2008); McLinden et al. (2014); Kharol et al. (2015); Griffin et al. (2019); Cooper et al. (2020), surface concentrations from satellite observations are estimated by scaling the satellite column measurements (VCD$_{\text{sat}}$) by the model ratio of the surface concentration (C_{model}) and tropospheric columns (VCD$_{\text{model}}$) at the coincident time and location:

$$C_{\text{sat}} = \text{VCD}_{\text{sat}} \times \frac{C_{\text{model}}}{\text{VCD}_{\text{model}}} \qquad (1)$$

Because the GEM-MACH operational model currently does not contain free tropospheric emissions such as from aircraft or lightning, we add a monthly mean from GEOS-Chem as the free tropospheric VCD to the GEM-MACH VCDs (further details in Griffin et al., 2019). These free tropospheric VCDs from GEM-MACH are on the order of 10^{14} molec. cm^{-2} (as a comparison, VCDs in polluted areas are on the order of 10^{16} molec. cm^{-2}).

3 Results

3.1 Validation and importance of parameters

Similar to previous studies, e.g. Long et al. (2022) we use 2022 to to assess the performance of the random forest algorithm to predict the surface concentration, and used the 2018–2021 dataset for training, where $R^2_{\text{training}} = 0.77$ and
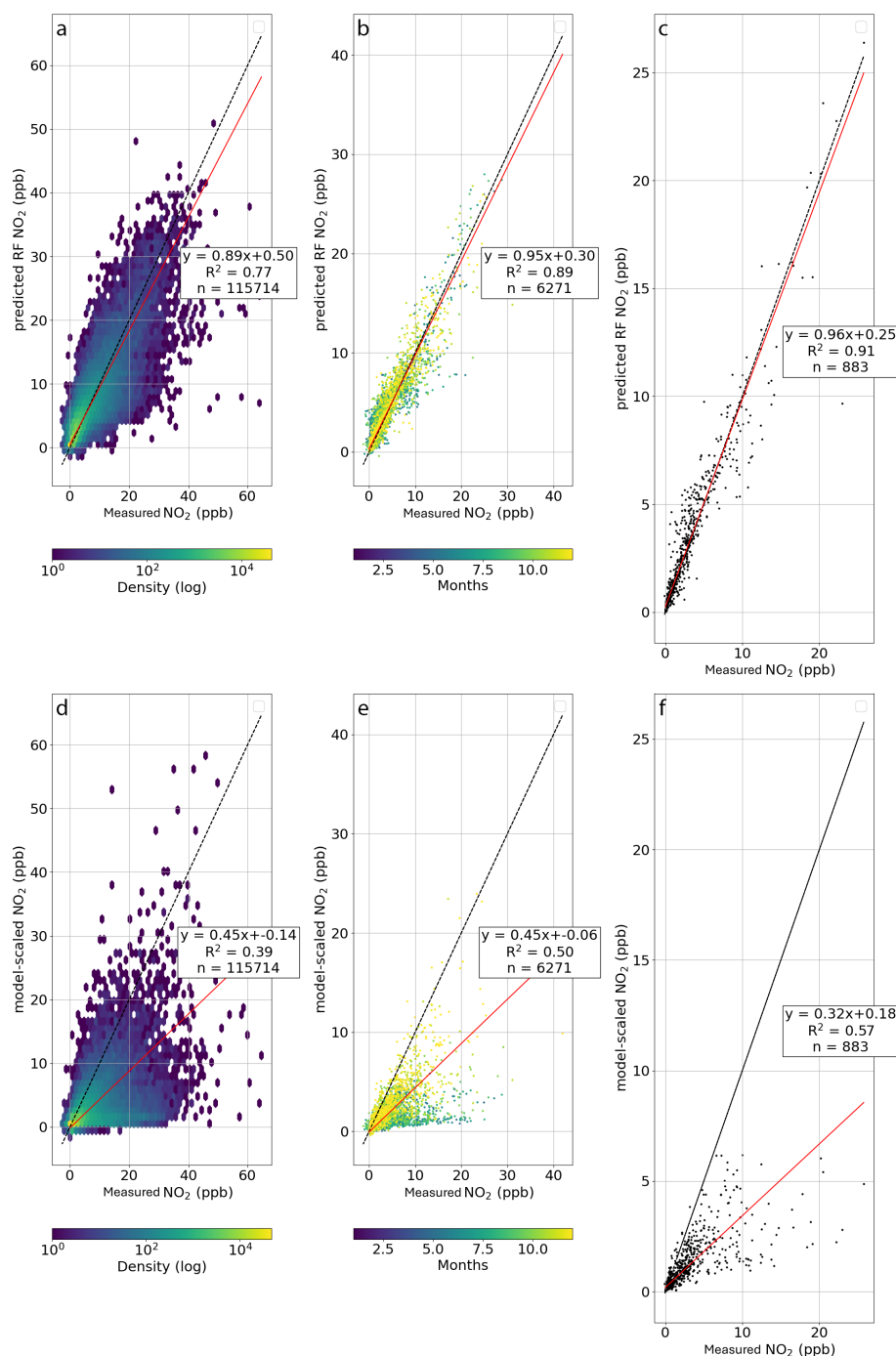
Figure 2. Validation for the 2022 dataset showing **(a)**, **(b)** and **(c)** for the random forest approach for daily, monthly and annual concentrations. The model scaling method for the same data points is shown in **(d)**, **(e)** and **(f)** for daily, monthly, and annual concentrations.

$R^2_{2022} = 0.77$. The result is shown in Fig. 2a for the random forest approach and Fig. 2d shows the same dataset using the traditional scaling approach. Each point represents a single overpass pixel (mid-day) and location. The random forest approach shows significant improvement ($R^2 = 0.79$) compared to the traditional ($R^2 = 0.38$) approach. Estimating annual or monthly means will increase the correlation fur-

ther. Monthly means are shown in Fig. 2b and e for the random forest and traditional scaling, respectively. Averaging the datasets increases the R^2 for both the machine learning ($R^2 = 0.89$) and the traditional scaling, however, the low bias in the traditional scaling remains and the R^2 only reaches 0.5. The annual means for each station are shown in Fig. 2c and f. While the traditional approach predicts much lower
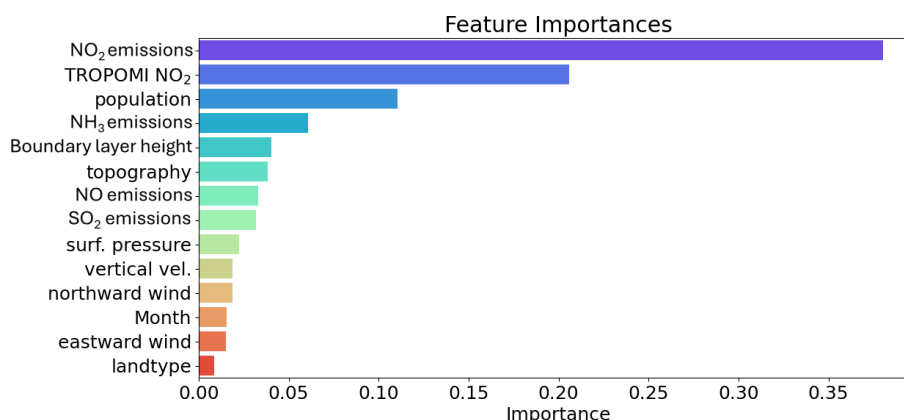
Figure 3. Importance of the input parameters for the random forest predictor.

values, the random forest surface concentrations are close to the 1-to-1 line.

Similarly it is important to assess the importance of each input parameter used by the random forest function. The results of the feature importance (obtained through an in-built function of sklearn "feature_importances_") are shown in Fig. 3 showing that the TROPOMI tropospheric column measurements are among the most important parameters for the prediction of the surface NO$_2$ concentrations.

3.2 Limitation and improvements in remote areas

As mentioned briefly, we filled in NO$_2$ surface concentrations from the GEM-MACH model in remote areas for our training dataset. Ground stations from NAPS and AQS are typically installed in urban or populated areas. This can be problematic for machine learning algorithms, as the random forest predictor is only representative of its training data, which results in remote areas computing much higher surface concentrations are computed than there actually are, if this is not taken into account. Including model output in remote areas helps the random forest predictor to be able to predict low concentrations. Additionally, we tested weighting stations that are in non populated areas five and ten times more than other stations. This method did not work as well as including synthetic stations, the NO$_2$ surface concentrations in northern Canada were still too high even when rural stations are weighted more in the random forest training (see Fig. A4). To create the model artificial "station" points we first created a regular grid of 1° in latitude between 60 and 40° N by 3° in longitude between 126 and 60° W. Then any points with a population density higher than 0 (utilizing the Gridded Population of the World (GPW) dataset were removed, leaving 290 remote locations (as shown in Fig. 1) that are underrepresented by the NAPS and AQS datasets. This is roughly the same amount as the NAPS stations and in total accounts for just under one third of the entire dataset used for the training of the random forest predictor. This number was

determined to be reasonable as this is less than the number of measurement stations but a large enough collection to make an impact on the prediction in remote areas.

An example of the impact is shown in Fig. 4 for a remote CAPMoN (Canadian Air and Precipitation Monitoring Network) measurement station located at Pinehouse lake in northern Saskatchewan (55.51° N, 106.72° W). This station is not part of NAPS and thus was not part of the training dataset offering an excellent opportunity to evaluate estimated NO$_2$ surface concentrations in a remote area, note that the measurements have a detection limit of 0.09 ppbv. Figure 4a shows the measurement data in the 2019 summer (black dots). The estimated NO$_2$ concentrations are shown as blue squares when only NAPS and AQS stations are used for the training of the model, and as turquoise diamonds when the additional model "stations" are included in the training data. The results using the traditional scaling method are shown as purple points. Figure 4b shows estimated versus the measured surface concentrations for coincident data points. The current version utilizing the random forest predictor with NAPS, AQS and model surface concentrations as training data is the closest to the observations. This example highlights the high positive bias when only station measurements are used as random forest predictor. The RF model is unable to predict low concentrations due to lack of low concentration scenarios in the training data. Generally, the random forest model does not do well predicting extreme concentrations (high and low surface concentrations). Using the additional surface concentrations from the GEM-MACH model helps the prediction in remote areas where surface concentrations are typically low (see further discussion in the next section and Fig. 6). The traditional method seems to be reasonable in remote areas but tends to underestimate the measurements slightly and is not as good as the estimated surface concentrations using the current version of the random forest model that includes synthetic stations in rural areas. Furthermore, including these synthetic rural stations also helps improve the overall accuracy during low pollution levels, see
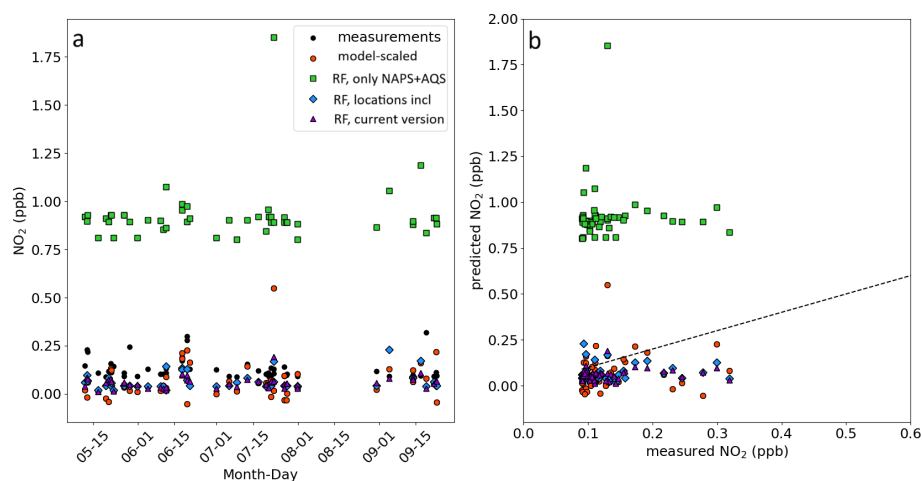
Figure 4. Comparison between measured and TROPOMI estimated NO$_2$ surface concentrations in the remote area Pinehouse lake (55.51° N, 106.72° W). The figure shows the correlation between the measured and estimated NO$_2$ for coincident measurements. Note that much higher concentrations up to 3 ppb were measured by the CAPMoN instrument, but these are not coincident with the TROPOMI overpasses.
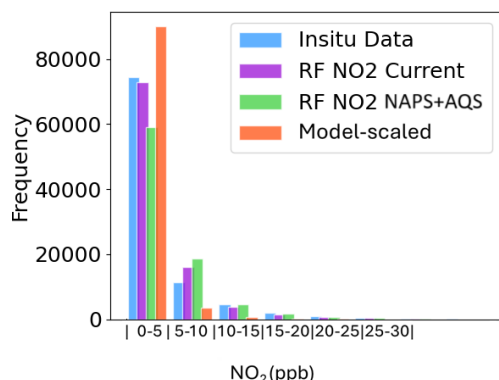

Figure 5. Frequency of surface concentrations for 2022 in 5 ppb bins, for "Insitu Data" from NAPS and AQS stations (blue), the current version of the RF model trained with synthetic stations in addition to the measurements (purple, "RF NO$_2$ current"), the RF model only using measurements (green "RF NO$_2$ no model"), and the traditional scaling method (organe, "traditional").

Fig. 5, shown is the frequency (illustrated in 5 ppb bins) of surface concentrations (compared to measurements "Insitu Data" shown as blue bars), when synthetic stations are not included the surface concentrations are often overestimated for surface concentrations less than 10 ppb, significant improvement is shown when the synthetic GEM-MACH stations ("RF NO$_2$ current") are included otherwise the RF surface concentrations are too high. The traditional method appears to have more frequent points on the lower end (0–5 ppb) compared to the actual measurements, showing that the traditional scaling method tends to under-predict the true surface concentrations.

3.3 Limitations and improvements to create maps

Figure 6 shows the estimated surface concentrations for the month of May 2023. Where the model was trained with data from 2018–2022. Figure 6a shows the current (best) version using AQS, NAPS and model for the training and eliminating the location with input parameters as listed in Table 2. For comparison the model scaled surface concentrations are shown in Fig. 6b, and are generally much lower than the random forest estimated values, especially in sub-urban and urban areas. Compared to the station measurements the traditional method is typically under-predicting and the current version of the random forest model shows are more similar pattern to the actual measurements (see Fig. 5). Figure 6c highlights the issue of over-predicting surface concentrations in remote areas when only NAPS and AQS are used for the training of the random forest predictor. Remote areas can show monthly average NO$_2$ surface concentrations of approximately 1 ppbv, but as high as 5 ppbv (e.g. over Greenland) which is not realistic. The next panel (Fig. 6d) shows the impact of using latitude and longitude in the training input parameters, the random forest predictor tries to interpolate between the locations resulting in sudden gradients across the map that are not realistic features. However, for specific measurement stations the correlation between the estimated and observed NO$_2$ is much improved when using location information as input parameters the correlation is better when using the location information in the RF model $R^2 = 0.8$, see Fig. A2, whereas the current version of the model only achieves ($R^2 = 0.77$), it depends on the purpose of the prediction: if the purpose is to fill in data gaps at specific stations better results are archived when latitudes and longitudes are included in the input parameters and the random forest is trained for the specific location. As can be seen
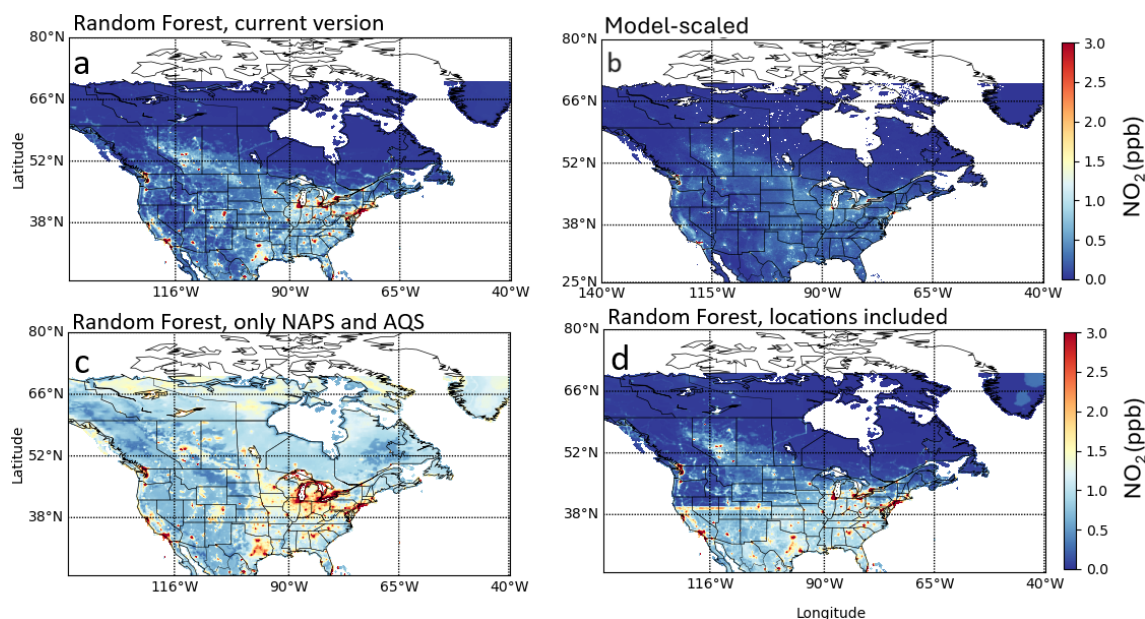
Figure 6. Monthly average of surface NO$_2$ concentrations for May 2023 over North America (binned on 0.1 with 0.2 oversampling). All figures have the same color scale. Panel **(a)** shows the current version of random forest estimated NO$_2$, panel **(b)** shows the model scaling NO$_2$ concentrations, panel **(c)** shows the random forest estimated NO$_2$ if only NAPS and AQS stations are used for the training, and panel **(d)** shows the random forest estimated NO$_2$ if locations (latitude and longitude) are included in the training data.

on the map, it is not advised to use location information for predicting locations not included in the training dataset as realistic maps cannot be estimated as the random forest model tries to interpolate between locations. Therefore, for predicting surface concentrations where no station measurements are available, locations data (longitude and latitude) should not be included in the training dataset of the random forest model.

3.4 Application examples and comparison to the traditional method

Lastly, this version of the NO$_2$ surface concentrations is a satellite level 2 product meaning they are derived on individual TROPOMI pixels. An example of a single satellite overpass is illustrated in Fig. 7 highlighting the improvement of the random forest predictor over the traditional scaling method. The original TROPOMI NO$_2$ VCDs are shown in Fig. 7a over the Greater Toronto Area (GTA) on 23 May 2023 (a clear-sky day), and no 2023 data has been used for the training of the random forest model. The NO$_2$ surface concentrations using the traditional scaling method and the random forest predictor are shown in Fig. 7b and c, respectively. The coincident measurements from the NAPS stations in this area are included as points (using the same color scale). This highlights the discrepancy of the traditional method that relies heavily on the model profiles and surface concentrations that are used for the scaling. The model profiles and surface concentrations are influenced by the location and magnitude

of emissions in the GEM-MACH model, the accuracy of the winds and the boundary layer heights. The traditional scaling method shows largest enhancement (of approximately 6.5 ppbv) north of Toronto in this example. It appears much lower than the coincident NAPS measurements. The random forest estimated surface concentrations correlate well with the location of the TROPOMI VCD enhancements and the enhancement measured by the NAPS station. The observations depict a realistic spatial picture of similar magnitude to the NAPS measurements. It should be noted that this was a clear-sky day and cloudy days will result in significant gaps due to low quality satellite observations, not all days compare quite as well to the NAPS measurements.

4 Results and Future Implications

To summarize, the random forest predictor has demonstrated significant advantages over traditional method of model profile scaling in predicting surface concentrations of NO$_2$ from TROPOMI NO$_2$ observations.

Improving the prediction of surface concentrations through machine learning involves a comprehensive approach that includes careful consideration of data sources, input parameters, hyperparameter tuning, and most importantly rigorous validation and testing. This is crucial to ensure that the machine learning model can accurately reflect the complex dynamics of the atmosphere and make realistic predictions without over-fitting.
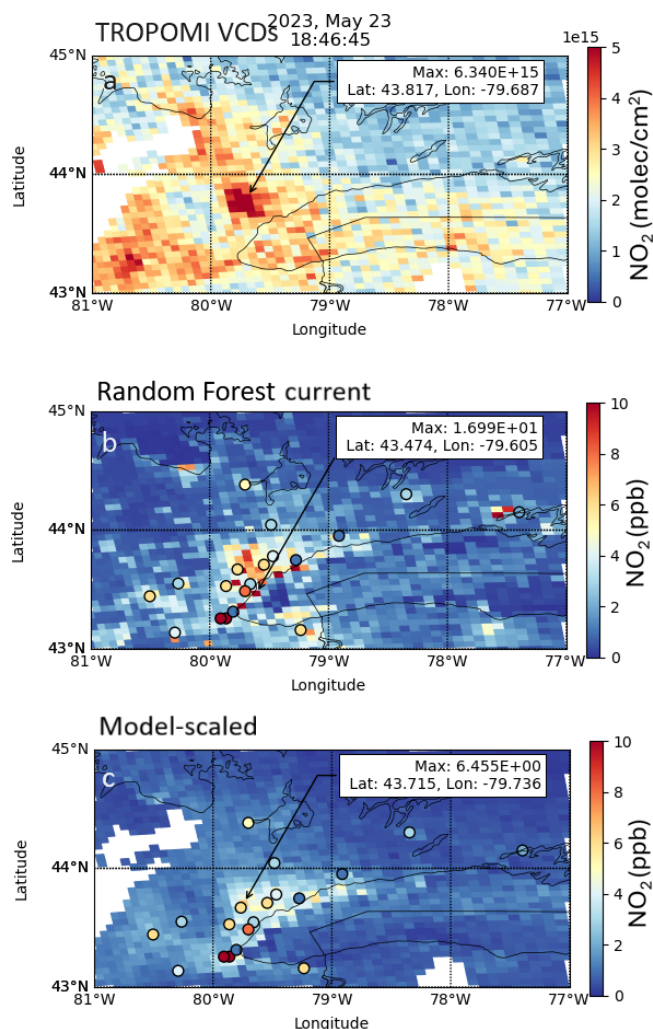
Figure 7. An example is shown a single overpass of the Toronto area on 23 May 2023, a clear-sky day. Panel **(a)** shows the TROPOMI VCDs, panel **(b)** shows the random forest estimated NO$_2$ concentrations, and panel **(c)** shows the model scaling NO$_2$ surface concentrations. Highlighted are the points with the greatest enhancement. The points shown in panel **(b)** and **(c)** are the coincident NAPS measurements on the same color scheme. For random forest training observations from 2018–2022 were considered (2023 is not included).

One of the key strengths of machine learning models is their excellent performance to fill in data measurement gaps, when location data is included in training. This allows for accurate predictions of concentrations in different years and is particularly useful in scenarios where ground-based instruments fail, face measurement gaps, or are decommissioned. Including the location information, however, limits the ability to predict the surface concentrations in unknown locations and can create odd gradients as the predictor tries to interpolate between locations.

Another important consideration is that surface stations often under-represent remote areas as they are typically in ur-

ban and polluted areas. This under-representation of remote areas can cause machine learning models such as the random forest predictor to over-predict concentrations when trained solely on available measurements. To overcome this limitation we trained the random forest machine learning, with additional model surface concentrations from ECCC's operational air quality forecast model in remote areas. This significantly enhanced the predictability of surface NO$_2$ concentrations across Canada and the US, including remote regions.

It should further be noted that the accuracy of these predictions is inherently tied to the quality of the training data. For example, if the chemiluminescence-based analyzers suffer from overestimation of NO$_2$ due to interference from PAN and nitric acid, the random forest estimated values will also overestimate the surface concentrations. The new satellite-derived surface NO$_2$ concentrations are complimentary to surface station monitoring as it relies on TROPOMI NO$_2$ VCD measurements to help fill in measurement gaps or areas that are currently unmonitored, which performs better than the traditional scaling method. The estimated values are typically better than using the model scaling method, but are still not flawless. Outliers are often challenging to predict, and the estimated surface concentrations show typically less spread and variation compared with the actual measurements. As an example, in 2022 there are 3 exceedances of NO$_2$ surface concentrations greater than 60 ppb for coincident dataset with TROPOMI, while the random forest predicted NO$_2$ surface concentrations were around 30–40 ppb. This is the case for all RF tests performed in this study. On-going validation with ground-based data remains essential. Furthermore, the models currently predict only mid-day surface concentrations, at the time of the TROPOMI satellite overpass.

In the near future, the random forest predictor can potentially be applied to observations from the geostationary Tropospheric Emissions: Monitoring of Pollution (TEMPO) satellite (Zoogman et al., 2017), which has the potential to create hourly daytime NO$_2$ surface concentration maps for North America.

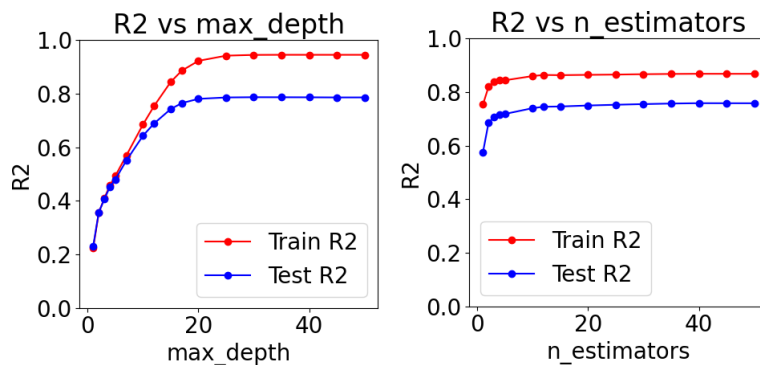## Appendix A: Tuning of the random forest model

Figure A1. Figure illustrating on how the optimal parameters for the random model were found. The max_depth and n_estimators were the most important parameters that needed tuning. The ideal point is found where the correlation of the training data is similar to the correlation of the test dataset. It is a sign of over-fitting if the correlation coefficient is much lower for the test dataset than for the training dataset, this is most common for a too large max_depth. N_estimators has a significant impact on speed.
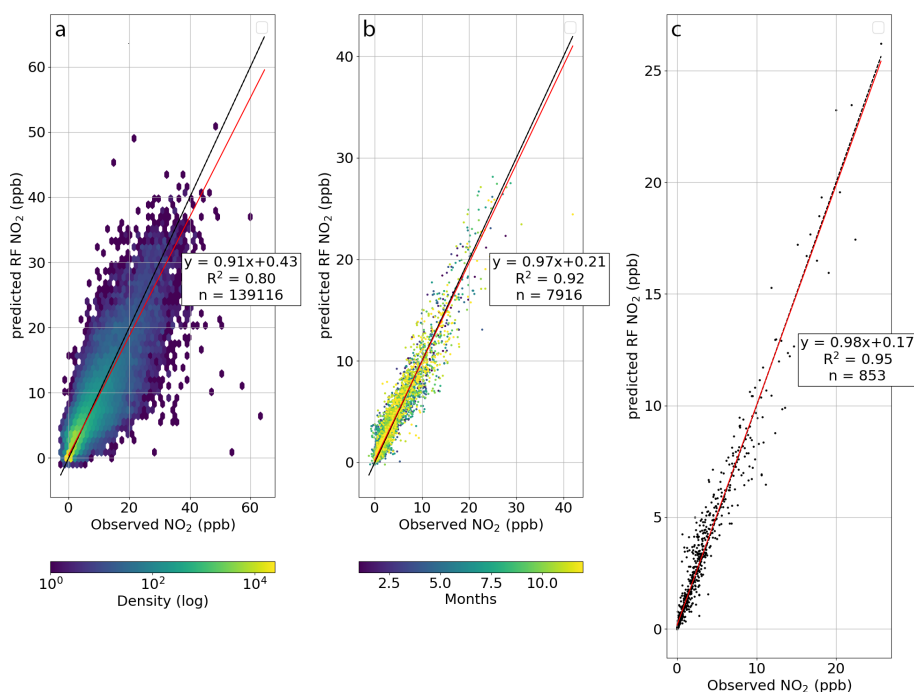
Figure A2. Same as Fig. 2 but using the location (latitude and longitude) as input parameters for the RF model. The overall correlation is better than the "current" version of the RF model, but when looking at a map (Fig. 6d) issues with this become apparent.
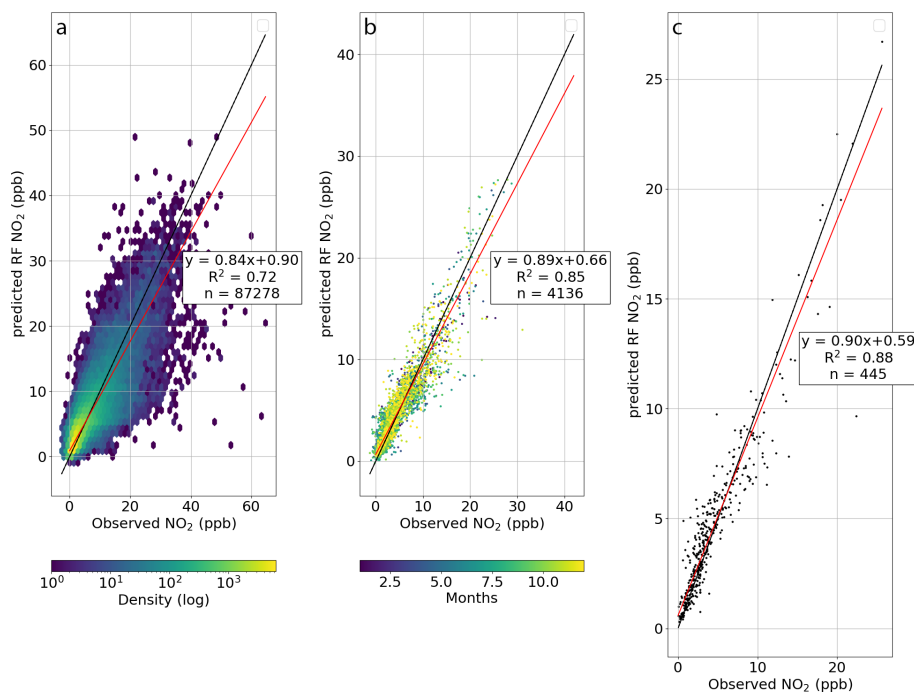
Figure A3. Same as Fig. 2 but only using only measurements from NAPS and AQS for the training of the RF model ("no model"). The values tend to be too high (see Figs. 5 and 4).
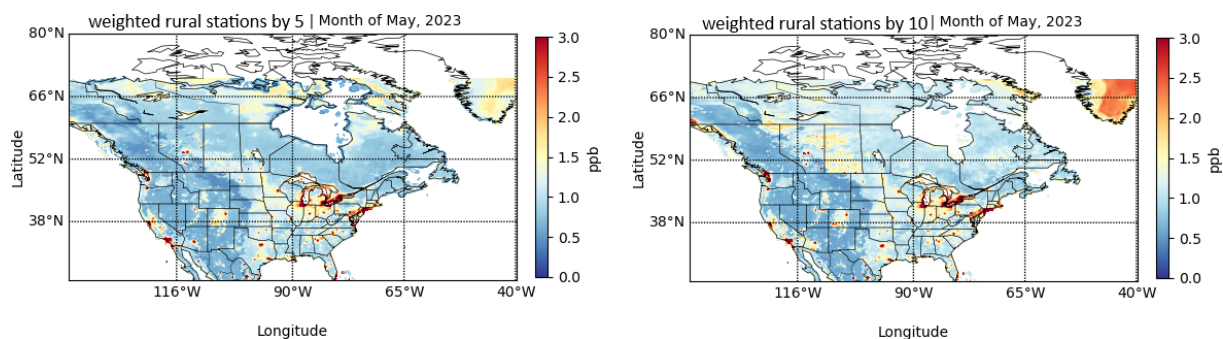
Figure A4. Same as Fig. 5 but training the RF model with NAPS an AQS measurements only. Stations with in a non-populated area are weighted 5 and ten times more than other stations.

References

Akingunola, A., Makar, P. A., Zhang, J., Darlington, A., Li, S.-M., Gordon, M., Moran, M. D., and Zheng, Q.: A chemical transport model study of plume-rise and particle size distribution for the Athabasca oil sands, Atmos. Chem. Phys., 18, 8667–8688, https://doi.org/10.5194/acp-18-8667-2018, 2018.

Beirle, S., Borger, C., Dörner, S., Li, A., Hu, Z., Liu, F., Wang, Y., and Wagner, T.: Pinpointing nitrogen oxide emissions from space, Science Advances, 5, eaax9800, https://doi.org/10.1126/sciadv.aax9800, 2019.

Breiman, L.: Random Forest, Machine Learning, 45, 5–45, https://doi.org/10.1023/A:1010933404324, 2001.

Chan, K. L., Khorsandi, E., Liu, S., Baier, F., and Valks, P.: Estimation of Surface NO$_2$ Concentrations over Germany from TROPOMI Satellite Observations Using a Machine Learning Method, Remote Sensing, 13, https://doi.org/10.3390/rs13050969, 2021.

Coats, C. J.: High-performance algorithms in the sparse matrix operator kernel emissions (SMOKE) modeling system, American Meteorological Society, Atlanta, GA, USA, proceedings of the Ninth AMS Joint Conference on Applications of Air Pollution Meteorology with AWMA, 28 January–2 February 1996, 1996.

Cooper, M. J., Martin, R. V., McLinden, C. A., and Brook, J. R.: Inferring ground-level nitrogen dioxide concentrations at fine spatial resolution applied to the TROPOMI satellite instrument, Environmental Research Letters, 15, 104013, https://doi.org/10.1088/1748-9326/aba3a5, 2020.

Copernicus Sentinel-5P (processed by ESA): TROPOMI Level 2 Nitrogen Dioxide total column products, Version 02, European Space Agency [data set], https://doi.org/10.5270/S5P-9bnp8q8, 2025.

Côté, J., Gravel, S., Méthot, A., Patoine, A., Roch, M., and Staniforth, A.: The Operational CMC–MRB Global Environmental Multiscale (GEM) Model. Part I: Design Considerations and Formulation, Monthly Weather Review, 126, 1373–1395, https://doi.org/10.1175/1520-0493(1998)126<1373:TOCMGE>2.0.CO;2, 1998.

Dee, D. P., Uppala, S. M., Simmons, A. J., Berrisford, P., Poli, P., Kobayashi, S., Andrae, U., Balmaseda, M. A., Balsamo, G., Bauer, P., Bechtold, P., Beljaars, A. C. M., van de Berg, L., Bidlot, J., Bormann, N., Delsol, C., Dragani, R., Fuentes, M., Geer, A. J., Haimberger, L., Healy, S. B., Hersbach, H., Hólm, E. V., Isaksen, L., Kållberg, P., Köhler, M., Matricardi, M., McNally, A. P., Monge-Sanz, B. M., Morcrette, J.-J., Park, B.-K., Peubey, C., de Rosnay, P., Tavolato, C., Thépaut, J.-N., and Vitart, F.: The ERA-Interim reanalysis: configuration and performance of the data assimilation system, Quarterly Journal of the Royal Meteorological Society, 137, 553–597, https://doi.org/10.1002/qj.828, 2011.

Demerjian, K. L.: A review of national monitoring networks in North America, Atmospheric Environment, 34, 1861–1884, https://doi.org/10.1016/S1352-2310(99)00452-5, 2000.

Dix, B., Francoeur, C., Li, M., Serrano-Calvo, R., Levelt, P. F., Veefkind, J. P., McDonald, B. C., and de Gouw, J.: Quantifying NO$_x$ Emissions from U.S. Oil and Gas Production Regions Using TROPOMI NO$_2$, ACS Earth and Space Chemistry, 6, 403–414, https://doi.org/10.1021/acsearthspacechem.1c00387, 2022.

Doxsey-Whitfield, E., MacManus, K., Adamo, S. B., Pistolesi, L., Squires, J., Borkovska, O., and Baptista, S. R.: Taking Advantage of the Improved Availability of Census Data: A First Look at the Gridded Population of the World, Version 4, Papers in Applied Geography, 1, 226–234, https://doi.org/10.1080/23754931.2015.1014272, 2015.

Environment Canada: Air pollution: drivers and impacts, https://www.canada.ca/en/environment-climate-change/services/environmental-indicators/air-pollution-drivers-impacts.html (last access: 12 June 2024), 2024.

Girard, C., Plante, A., Desgagné, M., McTaggart-Cowan, R., Côté, J., Charron, M., Gravel, S., Lee, V., Patoine, A., Qaddouri, A., Roch, M., Spacek, L., Tanguay, M., Vaillancourt, P. A., and Zadra, A.: Staggered Vertical Discretization of the Canadian Environmental Multiscale (GEM) Model Using a Coordinate of the Log-Hydrostatic-Pressure Type, Monthly Weather Review, 142, 1183–1196, https://doi.org/10.1175/MWR-D-13-00255.1, 2014.

Goldberg, D. L., Lu, Z., Oda, T., Lamsal, L. N., Liu, F., Griffin, D., McLinden, C. A., Krotkov, N. A., Duncan, B. N., and Streets, D. G.: Exploiting OMI NO$_2$ satellite observations to infer fossil-fuel CO$_2$ emissions from U.S. megacities, Science of The Total Environment, 695, 133805, https://doi.org/10.1016/j.scitotenv.2019.133805, 2019.

Goldberg, D. L., Anenberg, S. C., Kerr, G. H., Mohegh, A., Lu, Z., and Streets, D. G.: TROPOMI NO$_2$ in the United States: A Detailed Look at the Annual Averages, Weekly Cycles, Effects of Temperature, and Correlation With Surface NO$_2$ Concentrations, Earth's Future, 9, e2020EF001665, https://doi.org/10.1029/2020EF001665, 2021.

Goldberg, D. L., Tao, M., Kerr, G. H., Ma, S., Tong, D. Q., Fiore, A. M., Dickens, A. F., Adelman, Z. E., and Anenberg, S. C.: Evaluating the spatial patterns of U.S. urban NOx emissions using TROPOMI NO$_2$, Remote Sensing of Environment, 300, 113917, https://doi.org/10.1016/j.rse.2023.113917, 2024.

Griffin, D., Zhao, X., McLinden, C. A., Boersma, F., Bourassa, A., Dammers, E., Degenstein, D., Eskes, H., Fehr, L., Fioletov, V., Hayden, K., Kharol, S. K., Li, S.-M., Makar, P., Martin, R. V., Mihele, C., Mittermeier, R. L., Krotkov, N., Sneep, M., Lamsal, L. N., Linden, M. t., Geffen, J. v., Veefkind, P., and Wolde, M.: High-Resolution Mapping of Nitrogen Dioxide With TROPOMI: First Results and Validation Over the Canadian Oil Sands, Geophysical Research Letters, 46, 1049–1060, https://doi.org/10.1029/2018GL081095, 2019.

Griffin, D., Hempel, C., McLinden, C., Kharol, S. K., Lee, C., Fogal, A., Sioris, C., Shephard, M., and You, Y.: TROPOMI NO$_2$ surface concentrations python code, Zenodo [code], https://doi.org/10.5281/zenodo.17653066, 2025a.

Griffin, D., Hempel, C., McLinden, C., Kharol, S. K., Lee, C., Fogal, A., Sioris, C., Shephard, M., and You, Y.: TROPOMI NO$_2$ surface concentrations [data set], https://hpfx.collab.science.gc.ca/~deg001/surfaceNO2 (last access: 19 November 2025), 2025b.

Grzybowski, P. T., Markowicz, K. M., and Musiał, J. P.: Estimations of the Ground-Level NO$_2$ Concentrations Based on the Sentinel-5P NO$_2$ Tropospheric Column Number Density Product, Remote Sensing, 15, https://doi.org/10.3390/rs15020378, 2023.

Health Canada: Human Health Risk Assessment for Ambient Nitrogen Dioxide, https://www.canada.ca/en/health-canada/services/publications/healthy-living/human-health-risk-assessment-ambient-nitrogen-dioxide.html (last access: 12 June 2024), 2024.

Hu, H., Landgraf, J., Detmers, R., Borsdorff, T., de Brugh, J. A., Aben, I., Butz, A., and Hasekamp, O.: Toward Global Mapping of Methane With TROPOMI: First Results and Intersatellite Comparison to GOSAT, Geophysical Research Letters, 45, 3682–3689, https://doi.org/10.1002/2018GL077259, 2018.

Jeong, U. and Hong, H.: Assessment of Tropospheric Concentrations of NO2 from the TROPOMI/Sentinel-5 Precursor for the Estimation of Long-Term Exposure to Surface NO2 over South Korea, Remote Sensing, 13, https://doi.org/10.3390/rs13101877, 2021.

Kharol, S., Martin, R., Philip, S., Boys, B., Lamsal, L., Jerrett, M., Brauer, M., Crouse, D., McLinden, C., and Burnett, R.: Assessment of the magnitude and recent trends in satellite-derived ground-level nitrogen dioxide over North America, Atmospheric Environment, 118, 236–245, https://doi.org/10.1016/j.atmosenv.2015.08.011, 2015.

Lamsal, L. N., Martin, R. V., van Donkelaar, A., Steinbacher, M., Celarier, E. A., Bucsela, E., Dunlea, E. J., and Pinto, J. P.: Ground-level nitrogen dioxide concentrations inferred from the satellite-borne Ozone Monitoring Instrument, Journal of Geophysical Research: Atmospheres, 113, https://doi.org/10.1029/2007JD009235, 2008.

Lamsal, L. N., Martin, R. V., van Donkelaar, A., Celarier, E. A., Bucsela, E. J., Boersma, K. F., Dirksen, R., Luo, C., and Wang, Y.: Indirect validation of tropospheric nitrogen dioxide retrieved from the OMI satellite instrument: Insight into the seasonal variation of nitrogen oxides at northern midlatitudes, J. Geophys. Res., 115, D05302, https://doi.org/10.1029/2009JD013351, 2010.

Long, S., Wei, X., Zhang, F., Zhang, R., Xu, J., Wu, K., Li, Q., and Li, W.: Estimating daily ground-level NO$_2$ concentrations over China based on TROPOMI observations and machine learning approach, Atmospheric Environment, 289, 119310, https://doi.org/10.1016/j.atmosenv.2022.119310, 2022.

Makar, P., Gong, W., Hogrefe, C., Zhang, Y., Curci, G., Žabkar, R., Milbrandt, J., Im, U., Balzarini, A., Baró, R., Bianconi, R., Cheung, P., Forkel, R., Gravel, S., Hirtl, M., Honzak, L., Hou, A., Jiménez-Guerrero, P., Langer, M., Moran, M., Pabla, B., Pérez, J., Pirovano, G., José, R. S., Tuccella, P., Werhahn, J., Zhang, J., and Galmarini, S.: Feedbacks between air pollution and weather, part 2: Effects on chemistry, Atmospheric Environment, 115, 499–526, https://doi.org/10.1016/j.atmosenv.2014.10.021, 2015a.

Makar, P., Gong, W. F., Milbrandt, J., Hogrefe, C., Zhang, Y., Curci, G., Žabkar, R., Im, U., Balzarini, A., Baró, R., Bianconi, R., Cheung, P., Forkel, R., Gravel, S., Hirtl, M., Honzak, L., Hou, A., Jimenez-Guerrero, P., Langer, M., and Galmarini, S.: Feedbacks between air pollution and weather, Part 1: Effects on weather, Atmospheric Environment, 115, 2015b.

McLinden, C. A., Fioletov, V., Boersma, K. F., Kharol, S. K., Krotkov, N., Lamsal, L., Makar, P. A., Martin, R. V., Veefkind, J. P., and Yang, K.: Improved satellite retrievals of NO$_2$ and SO$_2$ over the Canadian oil sands and comparisons with surface measurements, Atmos. Chem. Phys., 14, 3637–3656, https://doi.org/10.5194/acp-14-3637-2014, 2014.

Moran, M. D., Ménard, S., Talbot, D., Huang, P., Makar, P. A., Gong, W., Landry, H., Gravel, S., Gong, S., Crevier, L.-P., Kallaur, A., and Sassi, M.: Particulate-matter forecasting with GEM-MACH15, a new Canadian air-quality forecast model, in: Air Pollution Modelling and Its Application XX, Springer, Dordrecht, the Netherlands, 2010.

National Air Pollution Surveillance Program: Hourly NO$_2$ surface concentrations, Government of Canada [data set], https://www.canada.ca/en/environment-climate-change/services/air-pollution/monitoring-networks-data/national-air-pollution-program.html (last access: 19 November 2025), 2025.

Pai, S. J., Heald, C. L., and Murphy, J. G.: Exploring the Global Importance of Atmospheric Ammonia Oxidation, ACS Earth and Space Chemistry, 5, 1674–1685, https://doi.org/10.1021/acsearthspacechem.1c00021, 2021.

Pendlebury, D., Gravel, S., Moran, M. D., and Lupu, A.: Impact of chemical lateral boundary conditions in a regional air quality forecast model on surface ozone predictions during stratospheric intrusions, Atmospheric Environment, 174, 148–170, https://doi.org/10.1016/j.atmosenv.2017.10.052, 2018.

Riess, T. C. V. W., Boersma, K. F., van Vliet, J., Peters, W., Sneep, M., Eskes, H., and van Geffen, J.: Improved monitoring of shipping NO$_2$ with TROPOMI: decreasing NO$_x$ emissions in European seas during the COVID-19 pandemic, Atmos. Meas. Tech., 15, 1415–1438, https://doi.org/10.5194/amt-15-1415-2022, 2022.

Russell, A. R., Valin, L. C., and Cohen, R. C.: Trends in OMI NO2 observations over the United States: effects of emission control technology and the economic recession, Atmos. Chem. Phys., 12, 12197–12209, https://doi.org/10.5194/acp-12-12197-2012, 2012.

Siddique, M. A., Naseer, E., Usama, M., and Basit, A.: Estimation of Surface-Level NO$_2$ Using Satellite Remote Sensing and Machine Learning: A review, IEEE Geoscience and Remote Sensing Magazine, 12, 8–34, https://doi.org/10.1109/MGRS.2024.3398434, 2024.

Steinbacher, M., Zellweger, C., Schwarzenbach, B., Bugmann, S., Buchmann, B., Ordóñez, C., Prevot, A. S. H., and Hueglin, C.: Nitrogen oxide measurements at rural sites in Switzerland: Bias of conventional measurement techniques, Journal of Geophysical Research: Atmospheres, 112, https://doi.org/10.1029/2006JD007971, 2007.

U.S. Environmental Protection Agency, Air Quality System Data Mart [data set], hourly NO$_2$ surface concentrations, https://www.epa.gov/outdoor-air-quality-data (last access: 19 November 2025), 2025.

Veefkind, J., Aben, I., McMullan, K., Forster, H., de Vries, J., Otter, G., Claas, J., Eskes, H., de Haan, J., Kleipool, Q., van Weele, M., Hasekamp, O., Hoogeveen, R., Landgraf, J., Snel, R., Tol, P., Ingmann, P., Voors, R., Kruizinga, B., Vink, R., Visser, H., and Levelt, P.: TROPOMI on the ESA Sentinel-5 Precursor: A GMES mission for global observations of the atmospheric composition for climate, air quality and ozone layer applications, Remote Sensing of Environment, 120, 70–83, https://doi.org/10.1016/j.rse.2011.09.027, 2012.

Winer, A. M., Peters, J. W., Smith, J. P., and Pitts, J. N. J.: Response of commercial chemiluminescent nitric oxide-nitrogen dioxide analyzers to other nitrogen-containing compounds, Environmental Science & Technology, 8, 1118–1121, https://doi.org/10.1021/es60098a004, 1974.

Zhang, J., Moran, M. D., Zheng, Q., Makar, P. A., Baratzadeh, P., Marson, G., Liu, P., and Li, S.-M.: Emissions preparation and analysis for multiscale air quality modeling over the Athabasca Oil Sands Region of Alberta, Canada, Atmos. Chem. Phys., 18, 10459–10481, https://doi.org/10.5194/acp-18-10459-2018, 2018.

Zoogman, P., Liu, X., Suleiman, R., Pennington, W., Flittner, D., Al-Saadi, J., Hilton, B., Nicks, D., Newchurch, M., Carr, J., Janz, S., Andraschko, M., Arola, A., Baker, B., Canova, B., Chan Miller, C., Cohen, R., Davis, J., Dussault, M., Edwards, D., Fishman, J., Ghulam, A., González Abad, G., Grutter, M., Herman, J., Houck, J., Jacob, D., Joiner, J., Kerridge, B., Kim, J., Krotkov, N., Lamsal, L., Li, C., Lindfors, A., Martin, R., McElroy, C., McLinden, C., Natraj, V., Neil, D., Nowlan, C., O'ullivan, E., Palmer, P., Pierce, R., Pippin, M., Saiz-Lopez, A., Spurr, R., Szykman, J., Torres, O., Veefkind, J., Veihelmann, B., Wang, H., Wang, J., and Chance, K.: Tropospheric emissions: Monitoring of pollution (TEMPO), Journal of Quantitative Spectroscopy and Radiative Transfer, 186, 17–39, https://doi.org/10.1016/j.jqsrt.2016.05.008, 2017.